Seasonal and inter-annual variability of western subtropical mode water in the South Pacific Ocean

Xiao Hua Wang · Vihang Bhatt · Youn-Jong Sun

Abstract The seasonal and inter-annual variability of the western subtropical mode water (hereafter STMW) in the South Pacific Ocean was examined using the Bluelink Re-ANalysis 2.1 (BRAN2.1) in terms of heat budget. The analysis of heat content change suggested that the seasonal cycle of surface heat flux played a dominant role in the formation of the STMW in the South Pacific Ocean. However, the surface heat flux and the East Australian Current (EAC) heat transport tended to compensate one another during STMW production. Out of phase or different amplitude of the components led to warming or cooling of the mixed layer, and the heat transport by the EAC in the formation of the STMW cannot be ignored. The correlation between volume anomalies of the STMW and net surface heat flux was insignificant, indicating that the inter-annual variability of the STMW was equally influenced by surface thermal forcing and ocean dynamic processes, such as horizontal advection. This study revealed the important role played by the EAC in the inter-annual variability of the STMW, i.e., a weakened heat transport by the EAC led to an increased volume anomaly of the STMW in the South Pacific Ocean. The STMW production can be further enhanced by La Nina, which drives positive anomaly in sea surface salinity in the western South Pacific and creates a favourable preconditioning for surface cooling in austral winter.

1 Introduction

Subtropical mode water (STMW) is the name given to a particular type of water mass feature observed in the subtropical oceans. It is described as a water mass with vertical homogeneity between the seasonal thermocline near the surface and the deeper main thermocline, and is of key importance in elucidating gyre circulation and climatic stability (Roemmich and Cornuelle 1992). It can also be viewed as the accumulation of a bulk of water nearest to the western boundary current (WBC) extension region, which is mainly generated by mixing and cooling during the winter season (Hanawa 1987; Roemmich and Cornuelle 1992). The name STMW is being used more extensively to describe various types of water mass found within subtropical gyre in the world's oceans (Talley 1999; Hanawa and Talley 2001; Joyce et al. 2009; Oka and Qiu 2012).

As a global feature, STMW is represented by different identities. It is described in the North Atlantic Ocean as the 18-degree water or as the North Atlantic STMW (NASTMW) (Worthington 1959). The temperature of the NASTMW decreases eastward to 17.5 degrees (Warran 1972). The STMW in the North Pacific Ocean has been described as a pycnostad between the seasonal and main pycnoclines in the subtropical gyre (Masuzawa 1969). It is formed on the warm side of the oceanic front in the Kuroshio and Kuroshio Extension (KE)

X. H. Wang · Y.-J. Sun
School of Physical Environmental Mathematical Sciences, UNSW Canberra at ADFA, Canberra ACT 2600, Australia

X. H. Wang (✉)
State Key Laboratory of Satellite Ocean Environment Dynamics, Second Institute of Oceanography, State Oceanic Administration, Hangzhou 310012, Peoples Republic of China
e-mail: hua.wang@adfa.edu.au

V. Bhatt
Now at Institute for Coastal Research, Max-Planck-Strasse 1, D-21502 Geesthacht, Germany

region during the winter period and is named the North Pacific STMW (NPSTMW). In this region, an intense winter cooling at the surface creates a thick mixed-layer depth (MLD). The deepening of MLD continues during the winter period and becomes the deepest at the end of the season (Bingham 1992). The distribution of mixed layer temperature shows a warming trend from west to east along the Kuroshio path (Suga and Hanawa 1990; Oka and Suga 2003).

Numerous observational and modelling studies for the North Pacific and North Atlantic STMWs have been conducted (Bingham 1992; Hautala and Roemmich 1998; Bates et al. 2002; Ladd and Thompson 2002; Krémeur et al. 2009; Nishikawa et al. 2010; Oka et al. 2011; Joyce 2012). On the other hand, the South Pacific Ocean is the widest body between the Australia (west) and the South American (east) land masses. The STMW in the eastern South Pacific (called SPESTMW) has been hypothesised to be a pycnostad remnant of the winter mixed layer in the eastern South Pacific, equatorward of the subtropical front where high salinity is expected to be the cause of deepened winter mixed layer (Tsuchiya and Talley 1996, 1998; Wong and Johnson 2003). The western South Pacific features the East Australian Current (EAC). The EAC is at its maximum during the summer period with an average southward geostrophic transport of 40 Sv, whereas its minimum average transport of 24 Sv appears during the austral winter (Ridgway and Godfrey 1997). Hence, the flow of the EAC is weaker than other western boundary currents, such as the Kuroshio and the Gulf Stream, and may lead to the weakness of the South Pacific Western STMW (hereafter SPWSTMW) thermostad, since its main thermocline has a shallower depth (Roemmich and Cornuelle 1992), and the Tasman front, which extends into the Southern Ocean subtropical gyre, similar to the extension of the thermal front along the KE into the North Pacific. The surface salinity south of the Tasman front decreases rapidly to 34.5 psu (Tomczak and Godfrey 1994).

Roemmich and Cornuelle (1992) was the first study that described both spatial distribution and temporal variability of the SPSTMW. They suggested that the weakness of the SPSTMW thermostad led to a shorter lifetime compared with the NPSTMW. Many studies followed, including Sprintall and Roemmich (1995), Roemmich et al. (2005), Hu et al. (2007), Tsubouchi et al. (2007) and Holbrook and Maharaj (2008). Roemmich et al. (2005) investigated the role of oceanic advection on mass and heat of the Tasman box based on eddy-resolving expendable bathythermograph (XBT) data during the period 1991–2002. They revealed that the STMW variability was influenced by the residual of oceanic heat advection in the study domain. Tsubouchi et al. (2007) illustrated that the SPSTMW was characterised by three types, with different spatial distributions and core layer temperatures, namely, the West, North and South types. Using synoptic CTD sections from the World Ocean

Circulation Experiment PR11 cruise data, Hu et al. (2007) investigated the existence of the STMW in the Tasman Front Extension around 29°S. It was observed in the depth range of 150–250 m with a temperature range of 16.5–19.5 °C. The vertical temperature gradient in the region was observed to be less than 1.6 °C per 100 m, and the potential vorticity was less than 2×10^{-10} m^{-1} s^{-1}. With the Digital Atlas of the Southwestern Pacific upper Ocean Temperatures (DASPOT) dataset for the period 1973–1988, Holbrook and Maharaj (2008) showed maps of the STMW thickness distribution. They used the criteria of a vertical temperature gradient of 2 °C per 100 m to identify the STMW in the region and found that the STMW extended across the entire width of the southwestern Pacific with a very broad swath ranging from the southeastern Australian coast to New Caledonia in the north. They also elucidated that the STMW volume varied seasonally, from 6.6×10^{14} m^3 in October (maximum) to 1.9×10^{14} m^3 in May (minimum). These observational studies provided vital information about the STMW in the region. However, they did not attempt to investigate the dynamic aspect of its seasonal and inter-annual variability that links to the local oceanographic processes, such as the EAC and its eddy activities, as the DASPOT dataset does not contain data such as current velocity measurements required to conduct such analysis. Therefore, dataset from an eddy-resolving ocean model would be advantageous to overcome deficient dynamic view on temporal–spatial variability of the SPWSTMW in previous papers.

A recent achievement of the Commonwealth Scientific and Industrial Research Organization, in collaboration with the Royal Australian Navy and the Bureau of Meteorology, is the Bluelink ReANalysis 2.1 (hereafter, BRAN2.1). It is assimilation modelling using an eddy-resolving ocean circulation model for the Australian region, which has provided a new and valuable synoptic dataset for this sparsely observed region. BRAN2.1 plays a key role in making a more sophisticated analysis of the relationship between oceanic circulation and of heat budget in the complex air–sea climate system. Furthermore, the better performance of BRAN2.1 was verified by analysing and comparing to other eddy-resolving ocean circulation models without data assimilation (Wang et al. 2013). The eddy-resolving model with data assimilation can realistically reproduce the structures of currents and fronts, and the mode water can therefore be understood dynamically with mesoscale features that are not fully covered by most observations (Oka and Qiu 2012). The purpose of this study is to comprehensively study the seasonal and inter-annual variability of the SPWSTMW off the east coast of Australia using BRAN2.1 dataset. The data and method used in this study are described in "Section 2". The seasonal variability and inter-annual variability of the mode water in the east Australian region are discussed in "Sections 3 and 4", respectively. Finally, main results are summarised in "Section 5".

2 Data and methods

The BRAN2.1 is the third version of BRAN, which depends on criteria of analysis periods and datasets used for assimilation in the global Ocean Forecasting Australian Model (OFAM; Schiller and Smith 2006; Schiller et al. 2008). The OFAM is based on the Modular Ocean Model (version 4; MOM4) (Griffies et al. 2004), which uses z-coordinate, hydrostatic assumption and primitive equations. The variable horizontal model grid (1,191×968 grid cells) is finer in the Asian–Australian region of 90°E–180°E 75°S–16°N, with a spatial resolution of 0.1° around Australia and gradually degrading to 2° in the North Atlantic Ocean. It has 47 levels in the vertical, which are equally spaced at 10-m interval above 250 m and subsequently increase exponentially with depth.

For reference, BRAN2.1 assimilates observations from satellite altimeters (ERS, GFO, TOPEX/Poseidon, Envisat and Jason-1) and 57 coastal tide gauges around Australia as well as sea surface temperature (SST) from Pathfinder for the period 1992–2002 and from AMSR-E for the period 2002–2006 along with in situ temperature data, e.g. Argo, Tropical Atmosphere–ocean (TAO), CTD and XBT. The daily BRAN2.1 reanalysis dataset for the period 1993–2006 was used for the current study. Monthly and annual averages for the region of 45°S–15°S, 150°E–180°E were extracted from the global dataset, which covers the SPWSTMW, and used for validation by the high-resolution expendable bathythermograph (HRX) data (Fig. 1).

The initial conditions for the OFAM were obtained by blending Levitus climatology (Levitus 2001) with the CSIRO Atlas of Regional Seas (CARS2000; Ridgway et al. 2002). The reanalysis was carried out using surface wind stress and surface heat flux from the European Center for Medium Range Weather Forecast (ECMWF) 40-Year Re-analysis (ERA-40; Uppala et al. 2005) data and from the operational forecasts of the ECMWF (Schiller et al. 2008); the latter was used as forcing in the OFAM every 6 h for the period of September 2002 onwards because the ERA-40 reanalysis was available only up to August 2002. The ERA-40 wind stress and flux data are available at 2.5°×2.5° spatial resolution, whereas the ECMWF operational forecast is available at much higher resolution (0.5°). To validate BRAN2.1, we used the Scripps Institution of Oceanography (SIO) HRX (http://www-hrx.ucsd.edu/index.html) transects along PX06 (Auckland–Suva), PX30 (Brisbane–Suva) and PX34 (Wellington–Sydney) as shown in the Fig. 1 (Roemmich et al. 2005).

Figure 1 shows the 14-year (1993–2006) mean temperatures from HRX transects (Fig. 1b) and BRAN2.1 (Fig. 1c). The isotherms of 14 and 20 °C are highlighted, as one of the criteria used to determine SPWSTMW thickness. The BRAN2.1 has steeper isotherms in the East Auckland Current region (Auckland–Suva section) but weaker and smoother EAC in the Sydney–Wellington section. A full evaluation of BRAN2.1 is beyond the scope of this article and has been
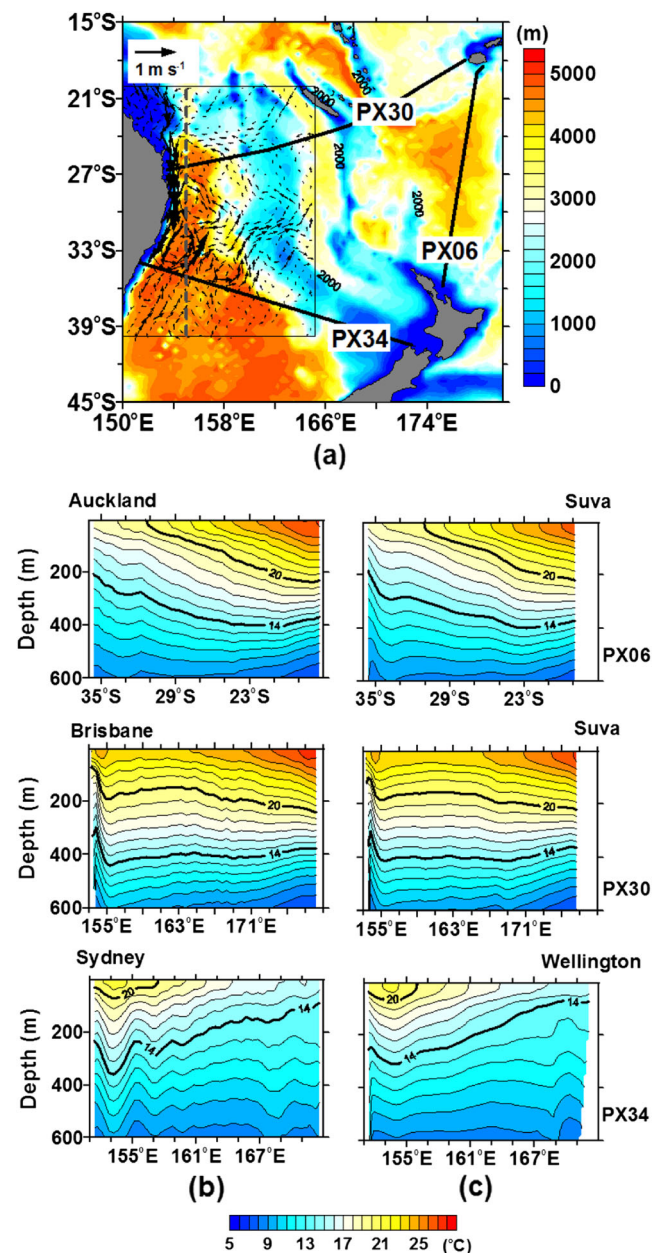
done by Oke and others (Oke et al. 2005; Schiller and Smith 2006; Oke and Schiller 2007; Oke et al. 2008; Schiller et al. 2008). The BRAN2.1 will be used to investigate oceanographic processes, such as heat budget and mode water thickness. In the later sections, we will also evaluate the quality of BRAN2.1 by comparing it to the results of Roemmich et al. (2005).

Fig. 1 **a** Map of the study area (20°S–40°S, 150°E–180°E), with bottom topography and the track lines (PX30, PX34 and PX06; *black lines*) of high-resolution expendable bathythermograph (HRX) transects. Vectors show monthly averaged surface velocities (in meters per second) in July from the BRAN2.1. The *dashed gray line* marks 155°E, and the *box* is the domain of the study. Vertical 14-year mean temperature sections from **b** HRX transects and **c** BRAN2.1. The *bold lines* show isotherms of 14 and 20 °C for the mode water in the present study

2.1 Definition of subtropical mode water in the South Pacific

A great advantage of BRAN2.1 is its uniform grid of 10-km resolution in the study region. However, such an advantage is missing for the vertical grid below 250 m. Therefore, the temperature and salinity data were interpolated linearly at 10-m intervals up to 1,000-m depth for the purpose of determining the SPWSTMW (hereafter STMW) thickness. It is important to note that the mode water is present between 150 and 250 m based on observational studies (Hu et al. 2007; Holbrook and Maharaj 2008).

Different studies use various criteria for identifying the STMW (Table 1) and apply different characteristic limits to define it. In the present study, the criteria used for determining mode water are a vertical gradient of 2 °C/100 m and a temperature range of 14 to 20 °C. In order to analyse the formation of the mode water, we will examine heat budget terms (heat advection, net surface heat flux and heat content change) in the STMW and then use these in finding any influence of ocean dynamics on the variability of the STMW. The STMW is generally defined as the water below the mixed layer, which is the water that has subducted and moved northward in the South Pacific. However, the mode water is connected to the mixed layer, and its heat content must be related to its formation in winter. Therefore, heat budget terms in the mixed layer will also be examined.

2.2 Mixed layer depth

Based on the extreme curvature of a temperature or density profile (Lorbacher et al. 2006), an empirical method has been devised to determine the MLD. In this approach, an emphasis is given to the second derivative (curvature) of the temperature or density profile. The MLD is determined in two steps. Firstly, the depth interval at which the MLD may be found is specified by two boundary conditions, which correspond to a significant gradient (>0.25 °C) and standard deviation (>0.02 °C) over 30 m below this level. Secondly, the MLD is determined based on the shallowest extreme curvature within the depth interval by finding the local extreme curvature and interpolating it to levels in the interval with either an exponential fit or a linear fit (Lorbacher et al. 2006). The empirical method has been shown to overcome the limitations of the gradient method, which is sensitive to the vertical resolution and vertical gradient of the profile at the base of the mixed layer and, therefore, was used to compute the MLD in this study.

3 Seasonal cycle of the mode water

As the STMW is a common feature observed in the oceans, similar mechanisms can be assumed for its formation, spreading and dissipation. It has been shown that winter cooling is important for the formation of the STMW in the North Atlantic Ocean, South Pacific Ocean and North Pacific Ocean (Bingham 1992; Holbrook and Maharaj 2008; Oka and Qiu 2012). Thus, the seasonal cycle of the STMW should be directly correlated with that of atmospheric forcing.

The STMW was calculated based on the criterion (2 °C/100 m and 14–20 °C) as mentioned previously. Figure 2 shows the seasonal variability of the STMW along 155°E using the monthly averages from 1993 to 2006. This meridian is preferred because it is in the segment of the West type classified by Tsubouchi et al. (2007) and also in the middle of the EAC extension region at 32°S. The cross-sections of the reanalysis temperature show that the MLD began to increase as early as April (upper 50–100 m) in the central Tasman Sea (along 155°E). The deepening of the mixed layer intensified during the austral winter (June to August); the onset of the STMW subduction after winter-time convective mixing could be visualised from July, and the subduction continued until November when the STMW had penetrated into the intermediate depth (at around 200 m). It can also been seen that the STMW was detached from the surface mixed layer after November.

The reanalysis also shows that the region within the isotherms of 14 and 20 °C along the eastern Australian coast shifted southward due to the seasonal heating (Fig. 2). The region of the STMW temperature range could be found near 40°S during this period (austral summer). During winter (June to August), reduced surface heating as well as weakening of the EAC shifted the STMW formation region northward, up to 32°S, in the surface, and the STMW was spread out northward along the 20 °C isotherm up to 28°S at 200 m depth (Fig. 2). It is interesting to note a 300-m water column of STMW between 100 and 400 m was present in November and December, and was separated from the STMW south of ~35°S. The STMW formation region was further elaborated using a spatial distribution of the STMW thickness for the southwestern Pacific in Fig. 3. The reanalysis revealed that the STMW thicknesses averaged in this region ranged between ~57 m in March (austral autumn) and ~182 m in September (austral spring). The growth of STMW thickness began as early as July near 30°S around Auckland and near 40°S around the southern coast of Australia; this can be visualised as a wide zonal band. As a distinct feature, the mode water, which was strongly subducted due to surface cooling in winter, could be found with an east-northward migration (Holbrook and Maharaj 2008). The formation of the STMW was intensified between 30°S and 35°S in October (Fig. 3). The intensified subduction in the formation region was observed to reach up as far east as 180°.

As an impact on the seasonal cycle of the STMW, the monthly averaged net surface heat flux (Q_{surf}) is shown in Fig. 4. The month of January exhibits extensive summer

Table 1 The criteria used to characterise the mode water

Source	Criterion for mode water		
	$\Delta T/\Delta Z$, (°C/100 m)	Temperature (T), (°C)	Planetary potential vorticity (PPV), ($\text{m}^{-1}\ \text{s}^{-1}$)
Wong and Johnson 2003	None	None	$<3\times10-10$
Hu et al. 2007	1.6	16.5 °C$<T<$19.5 °C	$<2\times10-10$
Holbrook and Maharaj 2008	2	14 °C$<T<$20 °C	None
Present study	2	14 °C$<T<$20 °C	None

heating in the ocean (~100 W m^{-2}), which can be seen south of 35°S in the Tasman Sea. Note that the Coral Sea in the north experienced relatively less warming (~50 W m^{-2}) during the same period. The Tasman Sea cooling began as soon as the austral autumn started. The panel for the month of April suggests that surface heat loss of more than 140 W m^{-2} appeared near 28°S and 35°S. The surface heat loss further intensified during winter. The surface heat flux for the peak winter month of June shows a large region of heat loss (>200 W m^{-2}) between 25°S and 40°S. The net surface heat flux in October (austral spring) suggests marginal cooling in the central Tasman Sea (~20 W m^{-2}). As the heat transport (by the EAC) into the Tasman Sea occurred, heat loss from ocean

to atmosphere and the timing of the transition from net cooling to net heating were not spatially uniform in October. In that month, the ocean was still being cooled due to latent heat loss in the western Tasman Sea while it received heat elsewhere. Therefore, the heat loss also increased with the strengthening of the EAC, which maintained a large air–sea temperature difference. The time series of the area averaged net surface heat flux suggests marginal heat gain (66 W m^{-2}) during the austral summer in comparison with the substantial heat loss (132 W m^{-2}) during the austral winter.

Figure 5 shows monthly averaged distributions of MLD. The MLD clearly began to deepen as early as April. In July, MLD of more than 100-m-thick broadly covered the Tasman

Fig. 2 Seasonal variability of the mode water along 155°E (see the *dashed line* in Fig.1a) based on the BRAN2.1. The contours show temperatures (units: degrees Celsius). The vertical temperature gradient is *shaded* to show the extent of the mode water (2 °C/ 100 m), and the *red curve* shows the mixed layer depth (units: meters). The *bold* contours show isotherms of 14 and 20 °C for the mode water in the present study
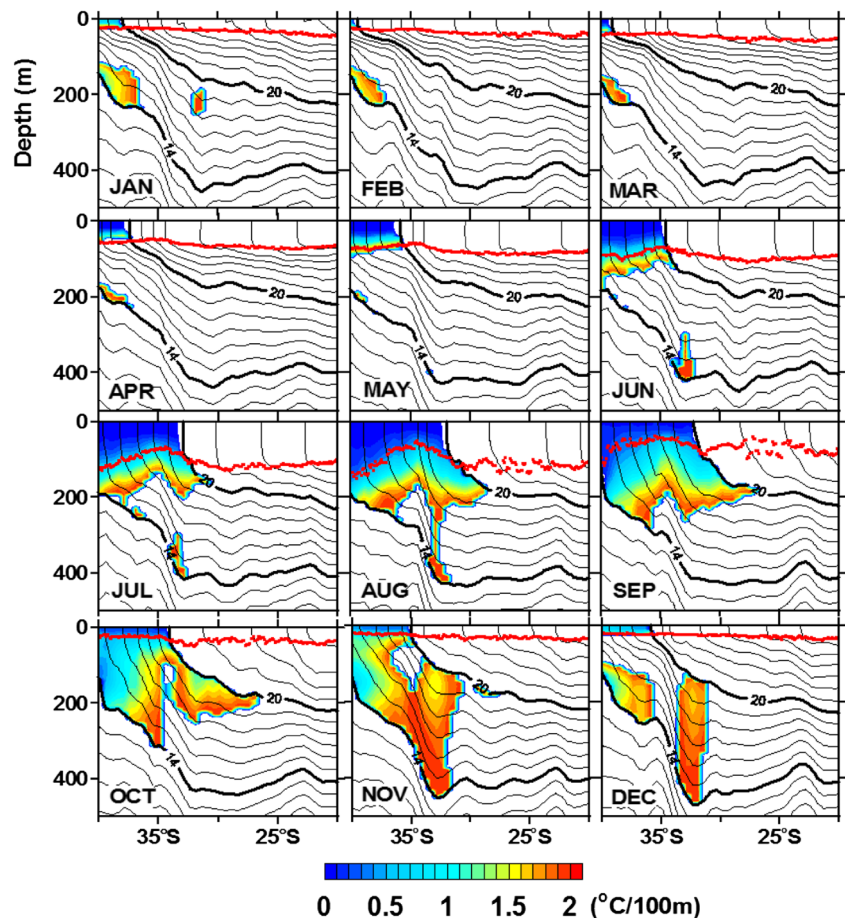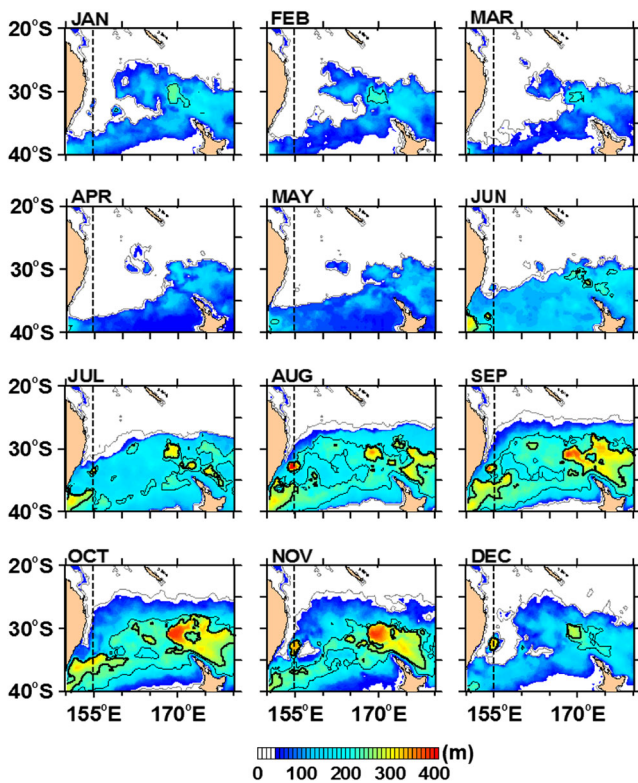
Fig. 3 Monthly averaged mode water thickness (units: meters) in the southwestern Pacific. The *gray lines*, *black thin lines* and *black bold lines* show 10-, 200- and 250-m thicknesses of the mode water, respectively. The *black dashed line* marks 155°E

Fig. 4 Spatial distribution of monthly net surface heat flux (units: watts per square meter) from the ERA-40. The *positive sign* indicates that the ocean gains heat from the atmosphere. The *black dashed line* marks 155°E

Sea. The formation of the STMW continued during the austral winter months (July to September) with the maximum MLD observed in August. The end of the formation and the beginning of the dissipation started in November as the mixed layer started to shoal. This continued during the austral summer months (January to March). It is important to note that the mode water formed during the austral winter persisted until the end of the austral summer.

The seasonal cycle of the total STMW integrated over the region (20°S–40°S and 150°E–180°E) suggests the mode water volume varied from 1.6 ($\pm$0.5)$\times$10^{14} m^3 in March to 7.8 ($\pm$0.5)$\times$10^{14} m^3 in September (Fig. 6). The total STMW volume obtained in the present study has a relatively larger range than that observed by Holbrook and Maharaj (2008), which was from 1.9×10^{14} m^3 in May to 6.6×10^{14} m^3 in October. It should be noted that the STMW definition used by Holbrook and Maharaj (2008) did not consider the mode water volume within the mixed layer that is applied in this study. However, the area of integration (20°S–40°S and 150°E–180°E) used here is smaller than that used by Holbrook and Maharaj (2008); also, the time periods used to prepare the STMW climatological cycle differ. Despite all these differences, the seasonal cycles shown by Holbrook and Maharaj (2008) and in this study are in good agreement.
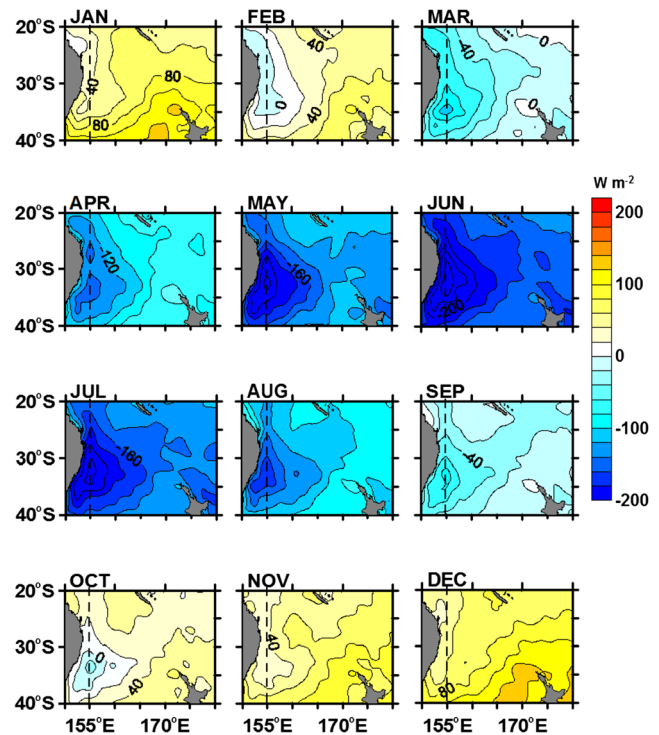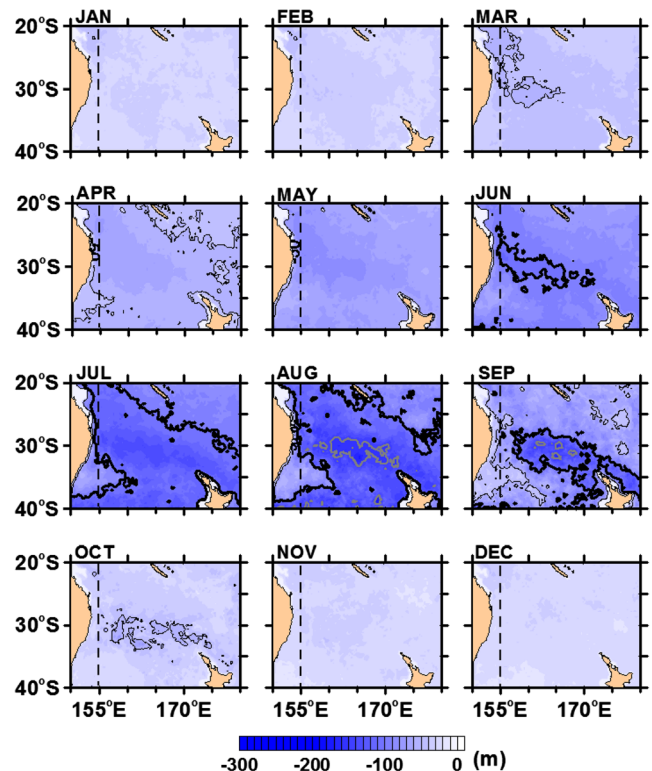

Fig. 5 Monthly averaged mixed layer depth. The contour interval is 50 m. The *black bold lines* and *gray bold lines* denote 100- and 150-m contours, respectively. The *black dashed line* marks 155°E

The seasonal variability of air–sea interaction and heat budget plays a significant role in the total STMW volume as shown in Figs. 3 and 4. Therefore, we calculated the heat budget (heat transport and heat content change) above 14 °C isotherm. The heat transport by the EAC across the northern open boundary also plays a key role in controlling the total heat transport. The heat transport (Q_{adv}) is computed using Eq. 1,

$$Q_{adv} = \int_l \int_{Z_{14}} \rho c_p v T dz dl + \int_A \rho c_p w T_{14} dA, \quad (1)$$

where ρ is the density of sea water, c_p is specific heat of sea water at constant pressure (joules per kilogram per degree Celsius), T is ocean temperature, Z_{14} is the depth of the 14 °C isotherm and v is the current velocity across the all open boundaries (denoted by l) of the study area (denoted by A). In the right-hand side of Eq. 1, the second term indicates the vertical heat transport across the surface of 14 °C isotherm (T_{14}). w is the vertical velocity at Z_{14}. The positive sign indicates that the heat is transported into the study area. The amount of the heat transport is averaged over the study area. As shown in Fig. 7, the heat transport became larger in the summer season when the EAC was the strongest. This heat transport variability is more remarkable between 150°E and 180°E E in the northern boundary (20°S) (not shown).

In addition, we calculated the heat content change (Q_{hc}) in the study area, which accounts for the heat gain or loss in the vertically integrated column during the period of ΔT, using Eq. 2,

$$Q_{hc} = \int_{Z_{14}}^0 \rho c_p \Delta T / \Delta t dz, \quad (2)$$

where ΔT is the temperature change over a given time Δt (1 month) and Z_{14} is the depth of the 14 °C isotherm. The heat content change averaged over the study area is shown in Fig. 7. The annual mean area averaged heat budget terms, such as net surface heat flux (−27.9 vs. −28.7 W m^{-2} for BRAN2.1 vs. Roemmich et al. (2005)), heat transport (49.7 vs. 42.3 W m^{-2}) compared fairly well, but heat content change (25.4 vs. 1.3 W m^{-2}) differs due to the fact that the latter used the observation data. Table 2 shows the relative roles of the heat budget terms averaged over the study area. It shows that the net surface heat flux is compensated by the heat transport by advection into the domain, resulting in a positive heat content change. It should be noted that the heat budget for BRAN2.1 is approximately closed. Although the heat content change was dominantly determined by the net surface heat flux (Fig. 7), the heat transport provided a balance in the heat budget closure in the STMW region. The relation between net
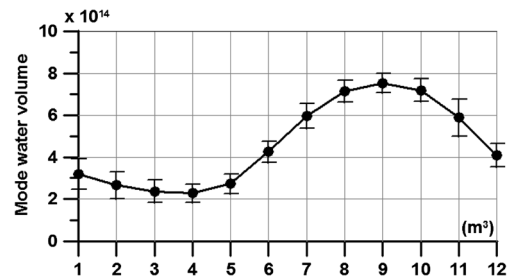

Fig. 6 Seasonal variability of the mode water volume (cubic meters). The error *bars* denote monthly mean standard deviations

surface heat flux (Q_{surf}) and ocean heat transport (Q_{adv}) tended to compensate one another (Fig. 7). Therefore, out of phase or different amplitude of the components led to the warming or cooling of the mixed layer. Time–integral storage is the cumulative sum of heat transport (Q_{adv}) and net surface heat flux (Q_{surf}). The time–integral storage was positive from December to May (austral summer and autumn), while that from June to November (austral winter and spring) was negative. The cooling that affected the formation of the mode water had a peak in August and September, corresponding to the maximum volume of the mode water (Fig. 7).

The formation of the STMW in the North Pacific was studied in detail by Bingham (1992). The author argued that the advection of warm water by the WBC extension plays a pivotal role in the STMW formation in the region. In the South Pacific, the warm water carried by the EAC during winter was cooled by the intense surface heat flux with a net loss. Under the influence of this intense heat exchange, the surface water became colder due to a shallow thermocline and weak convection. As the water left the EAC mainstream (see Fig. 1a for the path of the EAC), the mixed-layer thickness increased during the period from April to October (Fig. 5), and
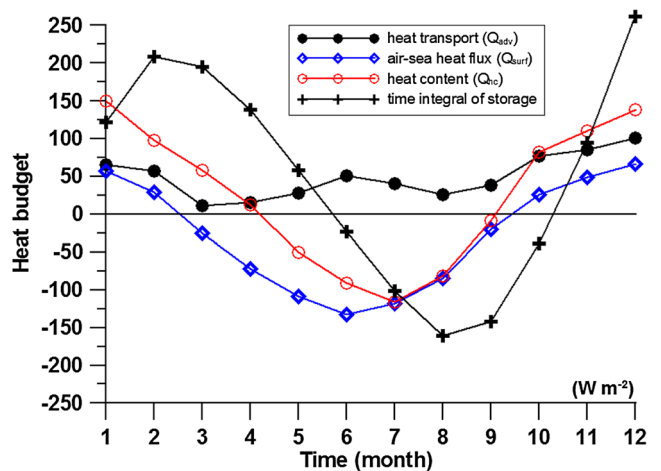

Fig. 7 Monthly-averaged heat budget into/out of the domain (20°S–40°S, 150°E–180°E). The *black line with solid circles* is heat transport, the *blue line with open diamonds* is net surface heat flux, the *red line with open circles* is heat content and the *black line with pluses* is time–integral storage that indicates the cumulative sum of heat transport (Q_{adv}) and net surface heat flux (Q_{surf})

Ocean Dynamics (2015) 65:143–154

Table 2 Annual mean heat budget averaged over the study area (150°E–180°E; 20°S–40°S). The positive (negative) sign represents that the heat is transported into (out of) the area. Q_{hc} denotes that heat content change in a given time (1 month), and Q_{surf} is net surface heat flux. Q_{adv} is heat transport across the study area. Units are in watts per square meter

	Q_{hc}	Q_{surf}	Q_{adv}
BRAN2.1	25.4	−27.9	49.7
Roemmich et al. (2005)	1.3	−28.7	42.3

formation of the STMW took place. Thus, it can be argued that the seasonal cycle of the EAC played a role in the STMW formation in the South Pacific (more discussion on this in "Section 4").

4 Inter-annual variability of the mode water

The vertical cross-section along 155°E is shown in Fig. 8 for the month of September, the end of winter period. It is the period when the mode water production reached its peak in a year. The figure shows a strong inter-annual variability in the
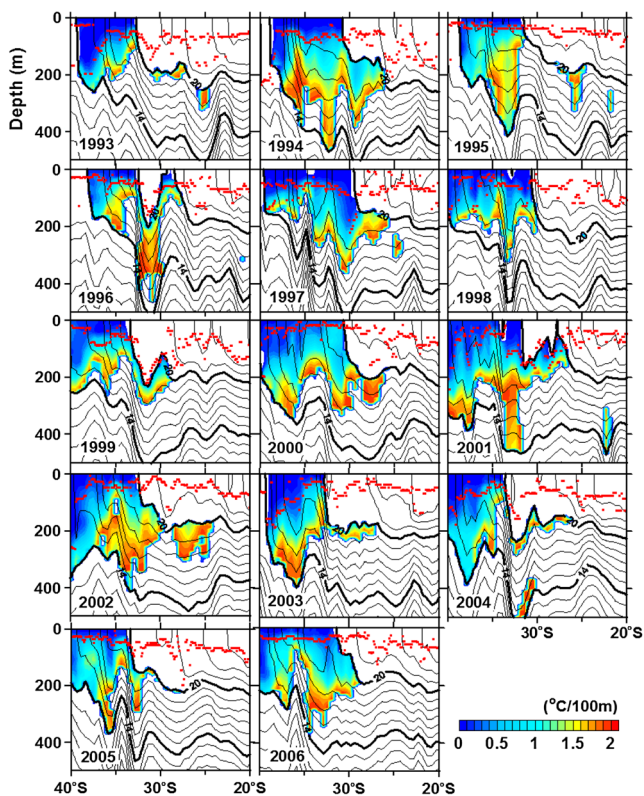
STMW. The formation area was located mainly between 40°S and 30°S where the maximum cooling was experienced during the winter period. The large volume of mode water at the cross-section appeared in the years 1994 and 2000–2002. In 2001 and 2002, the mode water was subducted up to 450 m and was advected equatorward along the 20 °C isotherm. Spatial distributions of the mode water thickness (Fig. 9) show that the mode water extended over a larger area during these 3 years compared with the other years. The mode water thickness was more extensive and deeper for the years of 1994 and 2000–2003 in the West type (150°E–160°E) and for the years of 1993–1997 in the East type (160°E–180°E). Holbrook and Maharaj (2008) analysed the observations of large volumes of the STMW in relation to the El Nino-Southern Oscillation (ENSO). They showed excessive thickening of the STMW in the western Tasman Sea during El Nino years. Thus, it can be argued that the anomalous cooling of the upper ocean during El Nino years increased the STMW formation across the region.

Fig. 8 Inter-annual variability in the mode water along 155°E during 1993–2006 for the month of September. The *contours* show isotherms (units: degrees Celsius). The vertical temperature gradient is *shaded* to show the extent of the mode water (2 °C/100 m), and the *red lines/dots* show mixed layer depth (units: meters). The *bold lines* show isotherms of 14 and 20 °C for the mode water in the present study
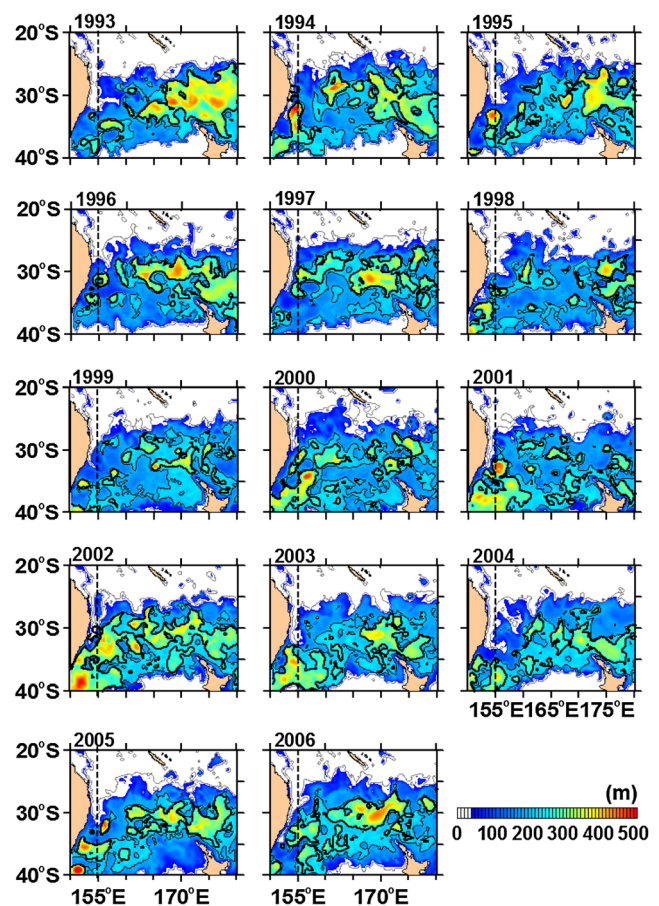

Fig. 9 Inter-annual variability of mode water thickness (units: meters) in the southwest Pacific Ocean for the period of 1993–2006. The mode water thickness shown is from the month of September. The *gray lines*, *black thin lines* and *black thick lines* show 10-, 200- and 250-m thicknesses of the mode water, respectively. The *black dashed line* marks 155°E

The Southern Oscillation Index (SOI) is generally used for determining the El Nino condition. The SOI for the period from 1993 to 2006 suggests that El Nino like conditions (−ve SOI) existed for the years 1993–1995 (moderate), 1997–1998 (strong), 2002–2003 (moderate) and 2004–2005 (weak) and that La Nina like conditions (+ve SOI) were present for the years 1995–1996 (weak), 1998–1999 (moderate), 1999–2000 (strong), 2000–2002 (weak) and 2005–2006 (weak) (bottom panels in Fig. 10).

The large spatial extents of the STMW thickness and volume can be explained using the argument of Holbrook and Maharaj (2008) for the years 1993–1997 and 2002–2003 in the East type (160°E–180°E). However, the STMW thickness in the West type (150°E–160°E) was relatively low even in the case of El Nino like conditions for the years 1993–1997 (Figs. 9 and 10). In addition, substantially larger volumes and more extensive spatial coverages in the West type occurred during the weak La Nina episode of 2000–2002, compared with those of moderate El Nino event in 2002–2003, suggesting that more complex physical processes other than El Nino events may drive the STMW variability in the region (West type).

Furthermore, as noted earlier, the seasonal maximum of the STMW volume occurred in September, with a value of 7.8×10^{14} m^3 (Fig. 6). The STMW volume anomalies were obtained by subtracting its seasonal cycle from the STMW volume. The largest STMW volume anomaly of up to 1.3×10^{14} m^3 was observed for the year 2002. It has already been argued that winter cooling due to surface heat loss plays an important role in the STMW formation. Although the inter-annual

contribution to the total surface heat flux signal cannot be ignored (not shown), the correlation was insignificant between the STMW volume anomaly and net surface heat flux anomaly ($R \sim −0.2$).

In order to identify the mechanisms driving the inter-annual variability, we divided the mode water formation into two regions (West and East types) along 155°E where the STMW formation is susceptible to the strength of the EAC (Tsubouchi et al. 2007). The time series from the seasonal cycle of anomalous STMW volume, area averaged thickness, air–sea heat flux, sea surface salinity (SSS), heat transport, and heat content change are shown in Fig. 10. It is clear that the STMW of the West type (left panels) had larger inter-annual variability than that of the East type (right panels). For the West type, the maximum STMW anomaly occurred in 2001–2003 and corresponded to a period with maximum SSS, minimum heat transport and net heat loss to the atmosphere. In contrast, a minimum STMW anomaly appeared from 1995 to 1998, with a large heat transport, heat gain from the atmosphere and a minimum SSS. The heat content change anomaly was negligible, despite the fact that both were El Nino years.

The mixed layer temperature plays an important role in determining STMW (e.g. Du et al. 2005). The temperature tendency (Tt) within the mixed layer can be divided into three terms: surface thermal forcing (Qt), horizontal advection (Av) and vertical entrainment (Et). The governing equation may be expressed as follows (Qu 2003; Du et al. 2005):

$$\frac{\partial T_m}{\partial t} = \frac{Q_0 - q_d}{\rho C_p h_m} - U \cdot \nabla T_m - \frac{w_{ent}(T_m - T_d)}{h_m}, \tag{3}$$

Fig. 10 Time series of anomalous (first rows) mode water volume, area averaged (second rows) mode water thickness, (third rows) air–sea heat flux, (fourth rows) sea surface salinity, (fifth rows) heat transport and (sixth rows) heat content change of the West (left panels) and East (right panels) types. The bottom panels are the SOI. The shaded areas represent the periods when the mode water thickness had the largest anomalies
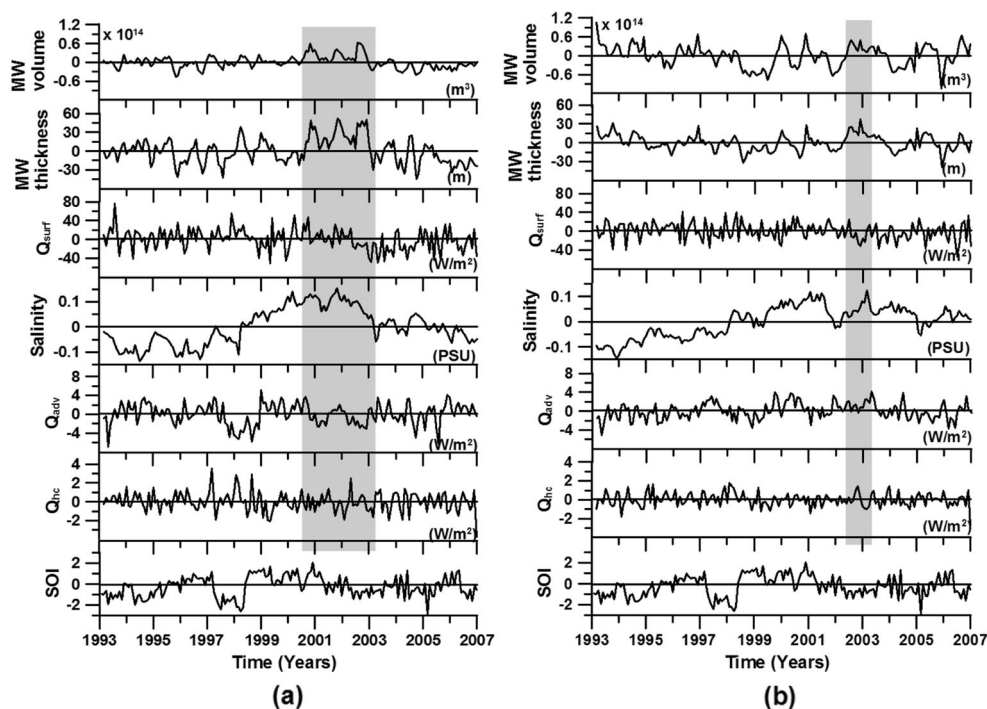
where T_m is mixed layer temperature, h_m is MLD and T_d is the temperature of water mass entrained at one model level below the mixed layer base. Q_0 is the net air–sea heat flux and q_d is the downward heat flux across the mixed layer base. q_d is computed as follows (Paulson and Simpson 1977):
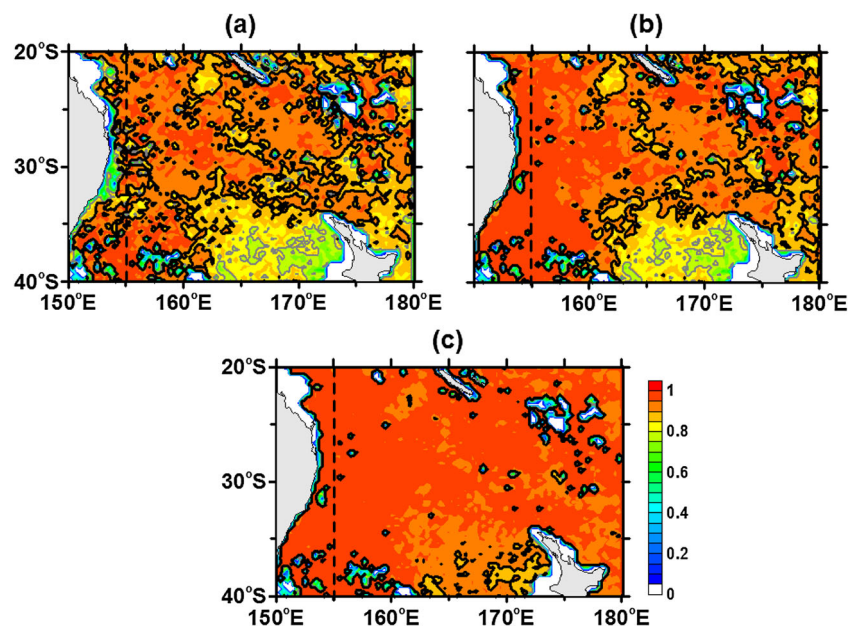
$$q_d = Q_r \left[R e^{-h_m/\xi_1} + (1-R) e^{-h_m/\xi_2} \right], \tag{4}$$

where Q_r is the shortwave radiation at the sea surface, and the values R, ξ_1 and ξ_2 are 0.58, 0.35 and 23, respectively (Du et al. 2005). The entrainment or detrainment rate in the heat budget for the mixed layer is derived as follows (Qu 2003):

$$w_{ent} = \frac{\partial h_m}{\partial t} + w_{mb} + U \ \nabla h_m \tag{5}$$

where $\partial h_m / \partial t$ is the rate of mixed layer deepening, w_{mb} is the velocity of water at the base of the mixed layer and $U \ \nabla h_m$ is the horizontal advection of water parcel below the mixed layer. The correlation between the temperature tendency (Tt) and each of the three terms on the right-hand side is calculated to evaluate which component in Eq. 3 controls the temperature of the mixed layer. The entrainment rate indicates the volume flux of the thermocline water cross the base of the MLD entering the mixed layer, that is, the deepening rate of the mixed layer, while the detrainment rate indicates the shrinking rate of the mixed layer (Qu 2003; Du et al. 2005). Figure 11 shows linear correlations between the temperature tendency (Tt) and surface thermal forcing (Qt), between Tt and the sum of surface thermal forcing and horizontal advection ($Qt+Av$), and between Tt and the sum of surface thermal forcing, horizontal advection and vertical entrainment ($Qt+Av+Et$).

Although the surface thermal forcing mainly controlled the temperature tendency ($R>0.8$ in Fig. 11a), the correlation was low in the region along the east coast of Australia where the EAC was dominant. Thus, the temperature tendency cannot be fully accounted for in Eq. 3 without adding the horizontal advection to the surface thermal forcing (Fig. 11b). These results further show that the EAC transport in the West type played an important role in the heat content change, thus the STMW formation process (Fig. 10a).

It is important to note that the STMW anomaly at the end of La Nina condition in 1998–2002 was the largest, larger than that of the strongest El Nino year of 1997 (Fig. 10). The Walin (1982) formulation for computing mode water formation showed a direct relationship between the STMW formation rate and SSS. In addition, the salinity maximum associated with evaporation led to buoyancy loss and retained the thickness of STMW after subduction (Tsuchiya et al. 1994; Hanawa and Talley 2001). Therefore, the role of SSS in the formation rate could not be discounted. During La Nina conditions, the SST around Australia was often warmer than normal while, during El Nino events, the SST was cooler than normal (Meyers et al. 2007). This warmer SST was associated with a higher rate of evaporation, which led to higher SSS. The SSS anomalies were noticed to be strongly negative during 1994–1997 and positive during 1998–2002. The negative anomaly during the El Nino years of 1994–1997 was, therefore, expected to provide less favourable conditions for local STMW formation and, hence, an overall low STMW volume. However, at the end of La Nina condition of 1998–2002, a strong positive anomaly of the SSS increased the formation rate, which may have resulted in its larger positive anomaly in the STMW volume in 2002 as shown in Fig. 10.

Fig. 11 Linear correlation **a** between temperature tendency (Tt) and surface thermal forcing (Qt), **b** between Tt and the sum of surface thermal forcing (Qt) and horizontal advection (Av), **c** between Tt and the sum of surface thermal forcing (Qt), horizontal advection (Av) and vertical entrainment (Et). In each panel, the gray and black bold contour lines denote the coefficient values of 0.8 and 0.9, respectively. The black dashed line marks 155°E

5 Summary

The seasonal and inter-annual variability of the STMW was investigated using the BRAN2.1 reanalysis and in relation to El Nino/La Nina events, along with the heat budget analysis (net surface heat flux, heat transport by the EAC and heat content change) of the mixed layer and mode water. The analysis of heat content change suggested that the seasonal cycle of net surface heat flux played a dominant role in the SPWSTMW formation. Meanwhile, the relation between surface heat flux and the EAC heat transport tended to compensate one another for the STMW production. Therefore, out of phase or different amplitude of the components led to the warming or cooling of the mixed layer, and the EAC heat transport in STMW formation cannot be ignored, as it provides a balance to surface atmospheric heat loss in the mixed layer heat content change.

Similarly, at the inter-annual scale, the STMW, in particular, the West type, was equally influenced by the surface heat flux and the heat transport associated with the EAC, but they did not act at the same time to compensate each other. Rather, these two components acted on the formation at different times, i.e. in different years, causing the inter-annual variability of the STMW. For example, the present analysis period covered several El Nino and La Nina events. The largest volume anomaly was noticed at the end of the La Nina period during 1998–2002. This was caused by a minimum heat transport associated with a weak EAC. The STMW production was further enhanced by positive anomaly in SSS that created a favourable preconditioning for surface cooling in winter. It should be noted that there were strong negative anomalies during the El Nino episodes of 1994–1997, with large heat transport (therefore stronger EAC). Therefore, ENSO events cannot be the sole process for representing large STMW volume anomalies.

References

Bates NR, Pequignet AC, Johnson RJ, Gruber N (2002) A variable sink for atmospheric CO_2 in subtropical mode water of the North Atlantic Ocean. Nature 420:489–493

Bingham FM (1992) Formation and spreading of subtropical mode water in the north Pacific. J Geophys Res 97(C7):11177–11189

Du Y, Qu T, Meyers G, Masumoto Y, Sasaki H (2005) Seasonal heat budget in the mixed layer of the southeastern tropical Indian Ocean in a high-resolution ocean general circulation model. J Geophys Res 110:C04012. doi:10.1029/2004JC002845

Griffies SM, Harrison MJ, Pacanowski RC, Rosati A (2004) A technical guide to MOM4. NOAA/Geophysical Fluid Dynamics Laboratory, GFDL Ocean Group Technical Report No. 5: 371pp

Hanawa K (1987) Interannual variation of the winter time outcrop area of subtropical mode water in the western North Pacific Ocean. Atmos Ocean 25(4):358–374

Hanawa K, Talley LD (2001) Mode waters. In: Siedler G, Church J, Gould J (eds) Ocean circulation & Climate: observing and modelling the global ocean. Academic Press, London, pp 373–386

Hautala SL, Roemmich DH (1998) Subtropical mode water in the Northeast Pacific basin. J Geophys Res 103:13055–13066

Holbrook NJ, Maharaj AM (2008) Southwest Pacific subtropical mode water: a climatology. Prog Oceanogr 77(4):298–315

Hu H, Qinyu L, Xiaopei L, Wei L (2007) The South Pacific subtropical mode water in the Tasman Sea. J Ocean Univ China 6(2):107–116

Joyce TM (2012) New perspectives on eighteen degree water formation in the North Atlantic. J Oceanogr 68(1):45–52

Joyce TM, Thomas LN, Bahr F (2009) Wintertime observations of subtropical mode water formation within the Gulf Stream. Geophys Res Lett 36:L02607. doi:10.1029/2008GL035918

Krémeur AS, Lévy M, Aumont O, Reverdin G (2009) Impact of the subtropical mode water biogeochemical properties on primary production in the North Atlantic: new insights from an idealized model study. J Geophys Res 114:C07019. doi:10.1029/2008JC005161

Ladd C, Thompson L (2002) Decadal variability of North Pacific central mode water. J Phys Oceanogr 32:2870–2881

Levitus S (2001) World Ocean Database. vol. 13, U.S. Department of Commerce. National Oceanic and Atmospheric Administration

Lorbacher K, Dommenget D, Niller PP, Kohl A (2006) Ocean mixed layer depth: a subsurface proxy of ocean–atmosphere variability. J Geophys Res 111:C07010. doi:10.1029/2003JC002157

Masuzawa J (1969) Subtropical mode water. Deep-Sea Res 16(5):463–468

Meyers G, McIntosh P, Pigot L, Pook M (2007) The years of El Nino, La Nina, and interactions with the Tropical Indian Ocean. J Clim 20:2872–2880

Nishikawa S, Tsujino H, Sakamoto K, Nakano H (2010) Effects of mesoscale eddies on subduction and distribution of subtropical mode water in an eddy-resolving OGCM of the western North Pacific. J Phys Oceanogr 40:1748–1765

Oka E, Qiu B (2012) Progress of North Pacific mode water research in the past decade. J Oceanogr 68:5–20

Oka E, Suga T (2003) Formation region of North Pacific subtropical mode water in the late winter of 2003. Geophys Res Lett 30(23):2205. doi:10.1029/2003GL018581

Oka E, Suga T, Sukigara C, Toyama K, Shimada K, Yoshida J (2011) "Eddy-resolving" observation of the North Pacific subtropical mode water. J Phys Oceanogr 41:666–681

Oke PR, Brassington GB, Griffin DA, Schiller A (2008) The Bluelink Ocean Data Assimilation System (BODAS). Ocean Model 20:46–70. doi:10.1016/j.ocemod.2007.11.002

Oke PR, Schiller A (2007) Impact of Argo, SST and altimeter data on an eddy-resolving ocean reanalysis. Geophys Res Lett 34:L19601. doi:10.1029/2007GL031549

Oke PR, Schiller A, Griffin GA, Brassington GB (2005) Ensemble data assimilation for an eddy-resolving ocean model. J R Meteorol Soc 131:3301–3311

Paulson CA, Simpson JJ (1977) Irradiance measurements in the upper ocean. J Phys Oceanogr 7:952–956

Qu T (2003) Mixed layer heat balance in the western North Pacific. J Geophys Res 108(C07):3242. doi:10.1029/2002JC001536

Ridgway KR, Dunn JR, Wilkin JL (2002) Ocean interpolation by four dimensional weighted least squares—application to the waters around Australia. J Ocean Atmos Tech 19(9):1367–1375

Ridgway KR, Godfrey JS (1997) Seasonal cycle of the East Australian Current. J Geophys Res 102(10):22921–22936

Roemmich D, Cornuelle B (1992) The subtropical mode waters of the South Pacific Ocean. J Phys Oceanogr 22:1178–1187

Roemmich D, Gilson J, Willis J, Sutton P, Ridgway K (2005) Closing the time-varying mass and heat budgets for large open areas: the Tasman Box. J Clim 18:2330–2343

Schiller A, Oke PR, Brassington G, Entel M, Fiedler R, Griffin DA, Mansbridge JV, Meyers GA, Ridgway KR, Smith NR (2008) Eddy-resolving ocean circulation in the Asian–Australian region inferred from an ocean reanalysis effort. Prog Oceanogr 76(3): 334–365

Schiller A, Smith N (2006) BLUELINK: Large-to-coastal-scale operational oceanography in the Southern Hemisphere, in Ocean Weather Forecasting: an integrated view of oceanography. Edited by Chassignet EP, Verron J, Springer International Press 427–439

Sprintall J, Roemmich D (1995) Regional climate variability and ocean heat transport in the southwest Pacific Ocean. J Geophys Res 100(C8):15865–15871

Suga T, Hanawa K (1990) The mixed layer climatology in the northwestern part of the North Pacific subtropical gyre and the formation area of the Subtropical Mode Water. J Mar Res 48(3):543–566

Talley LD (1999) Some aspect of ocean heat transport by the shallow, intermediate and deep overturning circulations. In: Mechanisms of global climate change and millennial time scales. P. Clark U, Webb RS, Keigwin LD (eds), Geophysical monograph series vol. 112 American Geophysical Union, Washington DC:1–22

Tomczak M, Godfrey JS (1994) Regional oceanography: an introduction. Pergamon Press, Oxford, p 422

Tsubouchi T, Suga T, Hanawa K (2007) Three types of South Pacific Subtropical mode waters: their relation to the large-scale circulation of the South Pacific Subtropical gyre and their temporal variability. J Phys Oceanogr 37:2478–2490

Tsuchiya M, Talley LD (1996) Water property distribution along an Eastern Pacific hydrographic section at 135°W. J Mar Res 54(3): 541–564

Tsuchiya M, Talley LD (1998) A Pacific hydrographic section at 88°W: water property distribution. J Geophys Res 103(C6):12899–12918

Tsuchiya M, Talley LD, McCartney MS (1994) Water-mass distributions in the western South Atlantic; a section from South Georgia Island (54S) northward across the equator. J Mar Res 52:55–81

Uppala SM, Kållberg PW, Simmons AJ, Andrae U, da Costa Bechtold V, Fiorino M, Gibson JK, Haseler J, Hernandez A, Kelly GA, Li X, Onogi K, Saarinen S, Sokka N, Allan RP, Andersson E, Arpe K, Balmaseda MA, Beljaars ACM, van de Berg L, Bidlot J, Bormann N, Caires S, Chevallier F, Dethof A, Dragosavac M, Fisher M, Fuentes M, Hagemann S, Hólm E, Hoskins BJ, Isaksen L, Janssen PAEM, Jenne R, McNally AP, Mahfouf JF, Morcrette JJ, Rayner NA, Saunders RW, Simon P, Sterl A, Trenberth KE, Untch A, Vasiljevic D, Viterbo P, Woollen J (2005) The ERA-40 re-analysis. Q J R Meteorol Soc 131(612):2961–3012

Walin G (1982) On the relation between sea-surface heat flow and thermal circulation in the ocean. Tellus 34(2):187–195

Wang XH, Bhatt V, Sun YJ (2013) Study of seasonal variability and heat budget of the East Australian Current using two eddy-resolving ocean circulation models. Ocean Dyn 63(5):549–563

Warran BA (1972) Insensitivity of the mode water characteristics to meteorological fluctuations. Deep-Sea Res 19(1):1–19

Wong APS, Johnson GC (2003) South Pacific eastern subtropical mode water. J Phys Oceanogr 33(7):1493–1509

Worthington LV (1959) The 18 degree water in the Sargasso Sea. Deep-Sea Res 5(2–4):297–305